Editors' Suggestion | Featured in Physics

Visualization of Elastic Flat Landau Rainbow

Yafeng Chen,[1,*] Zhihao Lan,[2,3] Xueyun Wen,[1] and Jie Zhu[1,4,†]
[1]Institute of Acoustics, School of Physics Science and Engineering, Tongji University, Shanghai 200092, China
[2]Department of Electronic and Electrical Engineering, University College London, London WC1E 7JE, United Kingdom
[3]College of Physical Sciences and Engineering, Mohammed VI Polytechnic University, Ben Guerir 43150, Morocco
[4]Shanghai Research Institute for Intelligent Autonomous Systems, Tongji University, Shanghai 201210, China

(Received 3 February 2026; revised 5 April 2026; accepted 2 June 2026; published 3 August 2026)

The Landau rainbow offers a promising way for advanced multiplexed wave processing. However, current Landau rainbows are restricted with narrow k-space range of flat Landau levels. Meanwhile, given the promise of rainbow trapping for developing multiplexed elastic devices in integrated phononic networks, the realization of flat Landau rainbow in elastic systems—particularly in the ultrasonic regime—remains highly desirable. Here, we realize megahertz Landau rainbows in an elastic metamaterial by artificially synthesizing both pseudomagnetic fields (PMFs) and pseudoelectric fields (PEFs). Importantly, nonuniform PMFs are introduced to enhance the k-space range of the flat zeroth Landau levels that form the Landau rainbow. Multiplexed megahertz ultrasonic energy trappings enabled by the Landau rainbow are directly visualized via laser scanning technology, which agree well with the simulation results. Moreover, the unique field distributions of such Landau rainbows are shown to result from the mode profiles of the Landau levels with different group velocities. Our Letter not only offers a new recipe for engineering the Landau rainbow from Landau levels with enhanced flatness, but also paves the way for the development of elastic integrated devices with multiplexed wave preprocessing capacities.

DOI: 10.1103/rt58-kxy9

Introduction—Landau levels, characterized by discrete energy levels that reveal the quantized localization behaviors of electrons under external magnetic fields [1], have played a pivotal role in advancing the development of topological physics in condensed matter systems [2–4]. As wave localizations in classical wave systems have important applications for developing novel devices, the concept of Landau levels has been recently transplanted into photonic, acoustic, and elastic crystals for achieving the efficient localization of electromagnetic, acoustic and elastic waves [5–29]. Unlike electrons, bosons such as photons or phonons in classical wave systems do not couple directly to real magnetic fields and therefore it is needed to artificially synthesize pseudomagnetic fields (PMFs) by engineering the structural geometry of the systems. Hitherto, diverse PMFs have been synthesized in two-dimensional (2D) classical wave systems. In elastic systems, by modifying the unit cells to engineer effective Dirac mass at fixed wave vectors, in-plane PMFs are synthesized, which further induce the chiral Landau levels [7–12], enabling the efficient high-throughput transportation of elastic waves with robustness. Meanwhile, by applying inhomogeneous strains to deform the lattices or modulating the unit cells in 2D lattices to shift the wave vector of Dirac points at fixed frequency, out-of-plane PMFs are constructed, which lead to the emergence of flat Landau levels [13–19], facilitating the resilient localization of elastic waves within a large area. However, current schemes of synthesizing out-of-plane uniform PMFs in elastic metamaterials constrain the shift of wave vector of the Dirac point within a narrow k-space range around the K/K' points, which further restricts the flat Landau levels to a narrow wave vector region, resulting in suboptimal flatness. It is desirable to explore new schemes of synthesizing out-of-plane PMFs to enhance the k-space range of flat Landau levels in elastic systems.

On the other hand, the Landau rainbow, where the flat Landau levels induced by the out-of-plane PMFs at different frequencies are separated into distinct spatial positions, can be generated by synthesizing additional pseudoelectric fields (PEFs), enabling the trapping of waves with different frequencies into distinct locations [30]. However, prior Landau rainbow in classical wave systems is restricted with narrow k-space range of flat Landau levels. It is thus meaningful to explore the new physical mechanism of the Landau rainbow to overcome such limitation. Meanwhile, given the promise of rainbow trappings for designing multiplexed elastic devices in integrated communication networks, realizing Landau rainbow in elastic systems, particularly in the megahertz ultrasonic regime, remains highly desirable [31–35], but which unfortunately has not been achieved yet.

*Contact author: yachen@tongji.edu.cn
†Contact author: jiezhu@tongji.edu.cn

 © 2026 American Physical Society

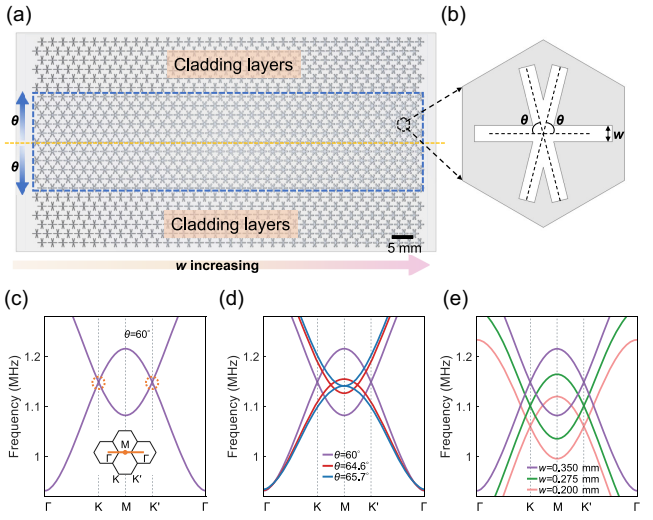


FIG. 1. Schematic of the elastic metamaterial and the band diagrams of the unit cells. (a) Schematic of the metamaterial, which is symmetric with respect to the yellow middle dashed line. (b) Schematic of the unit cell, where three rectangular slots with the same length and width are carved into an aluminum plate. Here, θ and w are two tunable parameters of the unit cell. (c) The band diagram of the unit cell with $\theta = 60°$ and $w = 0.14a$. The inset shows the reduced Brillouin zone and the high symmetry points. (d) The band diagrams of the unit cells with different θ. (e) The band diagrams of the unit cells with different w under $\theta = 60°$.

In this Letter, we achieve the Landau rainbow in an elastic metamaterial by synthesizing both out-of-plane PMFs and PEFs via gradient variations of two independent geometric parameters of the unit cell along both y and x directions. In particular, nonuniform PMFs via gradient variation along the y direction are introduced to enhance the k-space range of the flat Landau levels, whereas PEFs via gradient variation along the x direction separate the flat Landau levels at different frequencies into distinct locations, thus forming the Landau rainbow. Importantly, we show that the synergy between both the flat and non-flat parts of the Landau levels results in the unique field distribution of such Landau rainbow. Ultrasonic Landau rainbow with frequencies of around 1.1 MHz is experimentally confirmed, agreeing well with the simulation results. Our Letter suggests a recipe for constructing the Landau rainbows from Landau levels with enhanced k-space range of flatness in classical wave systems, paving the way for the development of advanced integrated elastic circuits for multiplexed ultrasonic signal processing.

The setup of the metamaterial—Figure 1(a) shows the schematic of the developed elastic metamaterial with the lattice constant of $a = 2.5$ mm, which is symmetric with respect to the middle dashed line and contains cladding layers at both the top and bottom to confine the energy of the Landau levels as the Landau levels are bulk modes, which without proper confinement can leak from the system boundaries. The unit cell as presented in Fig. 1(b) is made of an aluminium plate with the thickness of $t = 0.5$ mm, which is carved with three rectangular slots that share the same length (fixed as $0.85a$) and width. The inclination angle (θ) of two inclined slots of the unit cell and the width (w) of the slots serve as two independent geometric parameters, which, when modulated across the unit cells of the metamaterial, can be exploited to synthesize PMFs and PEFs, respectively. The elastic modulus, density and Poisson ratio of the aluminum plate are set as 70 GPa, 2700 kg/m^3, and 0.33, respectively. When $\theta = 60°$ and $w = 0.14a$, the unit cell is C_{6v} symmetric and two Dirac points are formed at the K and K' points of the band structure [36–38], as denoted by the red circles in Fig. 1(c). Note that in this Letter we only consider the out-of-plane polarized A_0 flexural modes, which can be effectively excited under the condition of out-of-plane excitation (see Sec. 1 of Supplemental Material [39]). The Hamiltonian of the Dirac cone could be written as $H_D = v_D(\hat{k}_x\sigma_x \pm \hat{k}_y\sigma_y)$, where v_D is the group velocity near the Dirac point, $\sigma_{x,y}$ are the Pauli matrices, $\pm$ correspond to the K/K' points, and $\hat{\boldsymbol{k}} = (\hat{k}_x, \hat{k}_y) = \boldsymbol{k} - \boldsymbol{k}_{K/K'}$ with $\boldsymbol{k}_{K/K'}$ representing the wave vectors of the K/K' points. To synthesize PMFs, we gradually modify θ to induce a gradient uniaxial lattice deformation. Specially, when $\theta > 60°$, the symmetry of the unit cell is reduced to C_{2v}, resulting in the shift of the Dirac point in momentum space from K (K') towards M (the Dirac cone is shifted to M when $\theta = 65.7°$ and will be gapped out beyond this value), as per Fig. 1(d). This shift of the Dirac cone in momentum space from K/K' toward M and eventual gapping out can be well captured by a tight-binding model (see Sec. 3 of Supplemental Material [39]). Moreover, by enlarging the width w of the slots (i.e., effectively decreasing the volume percentage of the aluminum in the unit cell), the frequency of the Dirac cone can be increased, as per Fig. 1(e), which can be exploited to introduce the PEFs.

The emergence of Landau levels with enhanced k-space range of flatness—The Hamiltonian of the shifted Dirac cone along K/K' to M [see the inset of Fig. 1(c) for the reduced Brillouin zone and the high symmetry points labeled] can be expressed as $H_D = v_D(\hat{k}_x - \delta k)\sigma_x + v_D\hat{k}_y\sigma_y$, where δk corresponds to the size of the shift and can be interpreted as the pseudomagnetic vector potential $\mathbf{A} = (\delta k, 0)$. Traditionally, the shift of the Dirac cone around K/K' is small and linear, which results in constant out-of-plane PMFs and flat Landau levels only in the vicinity of K/K' points. To generate Landau levels with enhanced k-space range of flatness, in this Letter we consider the shift of the Dirac cone from the full range of K/K' to M, which results in nonuniform PMFs and enhanced flatness around $k_x = 0$ (rather than the K/K' points). The supercell of the metamaterial with θ gradient along the y direction (consisting of 11 layers of unit cells within the blue shaded domain) is shown in Fig. 2(a). Note that in the supercell we also add cladding layers consisting of unit cells with

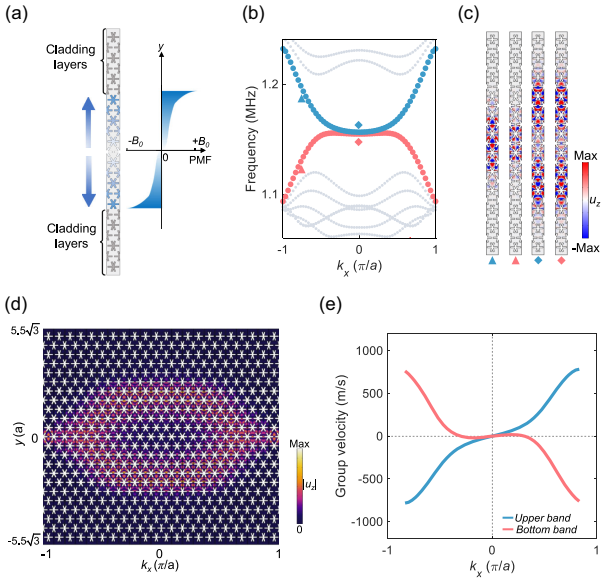


FIG. 2. The emergence of flat Landau levels around $k_x = 0$ induced by nonuniform PMFs. (a) Schematic of the supercell with symmetric gradient θ distributions along $+y$ and $-y$ directions (left panel) and the corresponding nonuniform PMF distributions (right panel, where the B_0 denotes the absolute out-of-plane PMF strength at $|y| = 2.5\sqrt{3}a$); the θ increases from 60° ($y = 0$) to 65.7° ($|y| = 2.5\sqrt{3}a$) with the interval of 1.12°. (b) The projected band diagram of the supercell in (a), which supports two nearly degenerate flat Landau levels around $k_x = 0$ with enhanced flatness extending a broader k-range. (c) The mode profiles of the Landau levels denoted by the different symbols in (b). (d) The evolution of the energy field distributions of the Landau levels denoted by the red points (bottom band) in (b) versus k_x. (e) The group velocity of the two zeroth Landau levels denoted by the red and blue points in (b).

bandgaps to confine the energy of the Landau levels, for which the detailed geometry parameters are given in Sec. 2 of Supplemental Material [39]. To generate the PMFs, we impose symmetric linear deformation $\theta(y) = 60° + \gamma|y|$ with θ increased along the blue arrows. The gradient of θ between adjacent layers is $\delta\theta = [(\theta_{\max} - 60°)/5]$, where $\theta_{\max} = 65.7°$. The induced out-of-plane PMFs under this setting, i.e., $B_z(y) = -[\partial A_x(y)/\partial y]$, are antisymmetric and nonuniform [$B_z(-y) = -B_z(y)$], as shown in the right panel of Fig. 2(a).

The projected band diagram of the supercell in Fig. 2(a) is shown in Fig. 2(b), from which we can observe the emergence of two nearly degenerate zeroth flat Landau level modes around $k_x = 0$, which occupy a broad k-space flat-band region (these two bands can also be seen from the tight-binding results in Secs. 3 and 4 of Supplemental Material [39]). Figure 2(c) shows that the eigenmode profiles of the two zeroth Landau levels denoted by the red and blue points are symmetric and asymmetric, respectively, with respect to the horizontal symmetrical line of the supercell [denoted by the yellow dashed line in Fig. 1(a)]. Meanwhile, the energies of the Landau levels at $k_x = 0$ (denoted by squares) are localized at the upper and bottom boundaries of the PMF domain, whereas they are localized at the central domain of the supercell when k_x is outside the flat region (denoted by triangles). Figures 2(d) and 2(e) further reveal that, when $|k_x|$ moves from π/a to zero (i.e., from the dispersive region to dispersionless region), the energy localization position gradually evolves from the central domain to the PMF boundaries, meanwhile the absolute group velocity decreases to zero gradually, indicating that the waves will stop propagating and become localized at the PMF boundaries. The zero group velocities and degeneracy of the zeroth Landau levels around $k_x = 0$ are due to the time reversal symmetry of the system. The emergence of Landau levels with enhanced k-space range of flatness around $k_x = 0$ and the evolution of energy localization position from the central domain to the PMF boundaries when $|k_x|$ moves from π/a to zero are also confirmed in the tight-binding model (see Sec. 3 of Supplemental Material [39]). Moreover, we would like to note that, compared with the zeroth flat Landau levels induced by the uniform out-of-plane PMF in elastic systems of prior works, the k-space range of flat bands in this Letter is greatly increased [15,16]. Meanwhile, as the number of unit cells within the supercell increases, the zeroth Landau levels become flatter with an enlarged k-space range, as demonstrated in Sec. 4 of Supplemental Material [39].

The emergence of elastic Landau rainbow under both PMFs and PEFs—The Landau rainbow requires that the frequencies of different Landau levels are separated into different spatial locations. As shown in Fig. 1(e), the frequency of the Dirac cone can be lifted continuously by increasing w, which implies that the frequencies of the two zeroth Landau levels in Fig. 2(b) can also be lifted continuously by increasing w. To demonstrate this, we show the projected band diagrams of the supercell with different w in Fig. 3(a), which indeed confirms the expectation and lays a solid foundation for the realization of the Landau rainbow. The gradual increase of the frequencies of the Dirac cone and Landau levels as w varies is equivalent to the effect of a PEF. To synthesize a uniform PEF and thus realize the Landau rainbow, we gradually increase w of the unit cells within the dashed box in Fig. 1(a) along the x direction from 0.2 to 0.35 mm, as denoted by the pink arrow. The corresponding effective Hamiltonian can be expressed as $H_D = E_x x\sigma_0 + v_D(\hat{k}_x - \delta k)\sigma_x + v_D\hat{k}_y\sigma_y$, with σ_0 being the identity matrix and E_x the synthetic electric field strength. The eigenfield profiles of the metamaterial in Fig. 3(b) demonstrate that elastic waves with different frequencies stop propagating at different locations, forming the Landau rainbow. In Sec. 3 of Supplemental Material [39], we further show the emergence of Landau rainbows in the tight binding model, which show very similar field distributions to these

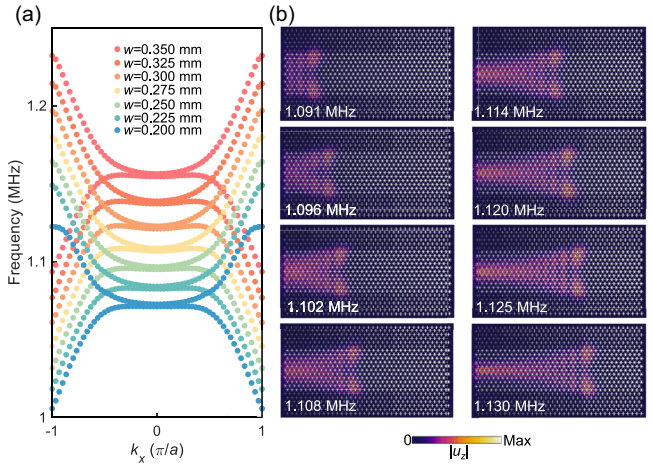


FIG. 3. The emergence of the Landau rainbow induced by both PMF and PEF. (a) The projected band diagrams of the supercell in Fig. 2(a) with different w. (b) The rainbow mode profiles of the elastic metamaterial in Fig. 1(a) with simultaneous θ gradient along y and w gradient along x at different frequencies.

obtained in the full-wave simulations of the metamaterial model, demonstrating that the mechanism to form such Landau rainbows could potentially be extended to elastic waves with other polarization modes or other classical systems as long as the wave vectors and frequencies of Dirac cones in these systems can be effectively engineered.

Moreover, the unique field distribution of the Landau rainbow, i.e., initially localized around the central domain and gradually stops propagating by spreading the energy to the top and bottom PMF boundaries, can be explained by the special dispersions of the two zeroth Landau levels as follows: the initial propagating modes correspond to the nonflat part around $k_x = \pm\pi/a$ with finite group velocity whose field distribution is around the central domain [see Figs. 2(b), 2(d), and 2(e)], and as they propagate and slow down, the flat modes around $k_x = 0$ gradually dominate whose field distribution is around the top and bottom PMF boundaries. As the modes at $k_x = 0$ have zero group velocity, the wave stops propagating and forms the Landau rainbow.

The experimental validation of the elastic Landau rainbow—To experimentally validate the Landau rainbow proposed above, we fabricate the elastic metamaterial [Fig. 4(a)] and scan its out-of-plane vibrational fields via a laser doppler vibrometer (for the experimental devices and the signal flow for characterizing the Landau rainbow, please see Sec. 7 of Supplemental Material [39]). To avoid boundary scatterings, the circumferences of the sample are coated with a high-stickiness bonding agent (Blu Tack). The captured out-of-plane vibration responses versus frequency at positions labeled by the points A–F in Fig. 4(a) are presented in Fig. 4(b), which show that the response peak of points A–F shifts rightward gradually in the frequency spectrum, consistent with the fact that larger

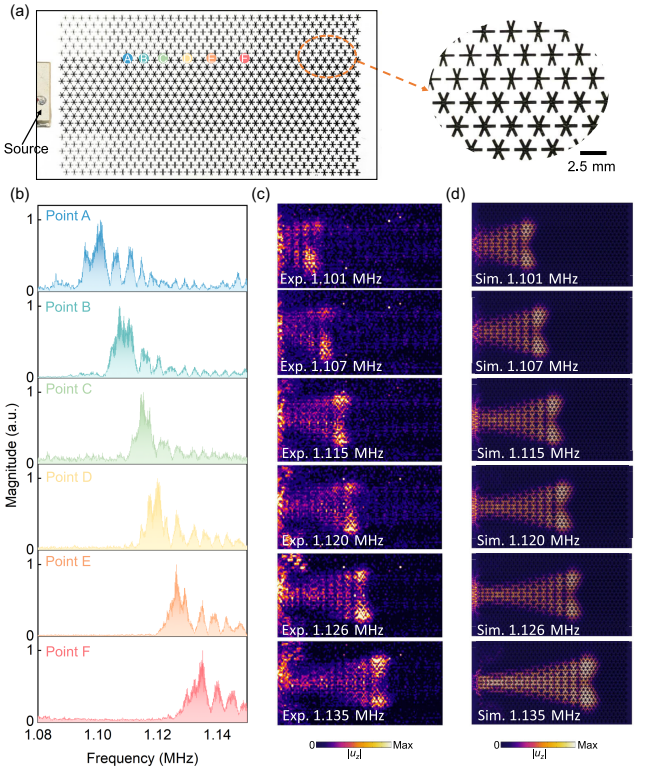


FIG. 4. The experimental validation of the Landau rainbow. (a) The schematic of the fabricated metamaterial sample (the w increases from $0.08a$ to $0.14a$ with the interval of $a/600$ from left to right), where the source and measurement locations A–F are marked. (b) The out-of-plane vibration responses versus frequency captured at different positions labelled by points A–F in (a). (c) The experimentally scanned field distributions corresponding to the frequencies of the response peaks in (b). (d) The simulated field distributions corresponding to the frequencies in (c) measured in experiment.

w toward the right end of the sample has higher frequency for the Landau levels. Meanwhile, the measured field distributions of the metamaterial, corresponding to the response peaks in the frequency spectra, demonstrate that ultrasonic waves with various frequencies (around 1.1 MHz) incident from the same position (note the source is located at the left end of the sample) stop at different positions as shown in Fig. 4(c), which move rightward with the increase of the frequency, providing a direct and compelling experimental evidence for the existence of ultrasonic Landau rainbow trapping in the proposed metamaterial system. The energy field distributions at the stop positions, localized at the top and bottom PMF boundaries, match well with the mode profiles of the flat Landau levels around $k_x = 0$. These measured field distributions also agree well with the simulation results given in Fig. 4(d). The slight difference of the stopping positions between experiments and simulations may come from the fabrication errors (see Sec. 6 of Supplemental Material [39]).

Conclusion and outlook—In summary, we have achieved the Landau rainbow in an elastic metamaterial by

constructing both out-of-plane PMFs and PEFs. The flatness and k-space range of the flat Landau levels that constitute the Landau rainbow are enhanced by the introduction of nonuniform PMFs. The Landau rainbow is visualized experimentally via the laser scanning technology, aligning well with the simulation results. The proposed scheme is also verified by tight-binding calculations, which indicates that the underlying mechanism to form such Landau rainbows does not depend on material details and thus could potentially be implemented in other classical wave systems as well, such as photonic and acoustic crystals. Meanwhile, compared with previous topological rainbow devices that confine energy to edges or corners with limited area, the developed elastic metamaterial supporting the Landau rainbow achieves high-flux and multiplexed ultrasonic energy trappings within the bulk, facilitating the development of advanced multiplexed ultrasonic communication systems. By integrating the metamaterial with multiple piezoelectric harvesters at the energy localization positions, it can be also exploited for rainbow ultrasonic energy harvesting [33]. Furthermore, the structural simplicity of our design supports further miniaturization, paving the way for the development of on-chip elastic integrated circuits with multiplexed functionalities [43–46].

Acknowledgments—This work is supported by the National Key R&D Program of China (Grants No. 2022YFA1404400 and No. 2022YFA1404403), the National Natural Science Foundation of China (No. 92263208 and No. 12102134), the Research Grants Council of Hong Kong SAR (No. AoE/P-502/20), and the Fundamental Research Funds for the Central Universities.

Data availability—The data that support the findings of this article are openly available [47].

[1] L. D. Landau, Diamagnetismus der metalle, Z. Phys. **64**, 629 (1930).
[2] K. von Klitzing, T.h Chakraborty, P. Kim, V. Madhavan, X. Dai, J. McIver, Y. Tokura, L. Savary, D. Smirnova, A. M. Rey, C. Felser, J. Gooth, and X. Qi, 40 years of the quantum Hall effect, Nat. Rev. Phys. **2**, 397 (2020).
[3] M. Z. Hasan and C. L. Kane, Colloquium: Topological insulators, Rev. Mod. Phys. **82**, 3045 (2010).
[4] Y. Li and C. Wu, High-dimensional topological insulators with quaternionic analytic Landau levels, Phys. Rev. Lett. **110**, 216802 (2013).
[5] L. Tao, Y. Liu, X. Zhou, L. Du, S. Ma, X. Yang, J. Zhang, Z. Li, K. Song, and X. Zhao, Inhomogeneous coupling induced quantized distribution of photonic states in Kagome lattices across different Landau levels, Commun. Phys. **8**, 24 (2025).
[6] Q. Mo, R. Zheng, C. Lu, X. Huang, Z. Liu, and S. Zhang, Observation of oriented Landau levels and helical zero modes in berry dipole acoustic crystals, Phys. Rev. Lett. **134**, 116604 (2025).
[7] K. Li, X. Zhang, Z. Zhang, Y. Cheng, and X. Liu, Observation of chiral Landau levels in a synthetic acoustic Weyl semimetal, Commun. Phys. **8**, 133 (2025).
[8] Y. Chen, Z. Lan, L. Fan, S. Liang, L. An, J. Zhu, and Z. Su, Realization of broadband ultrasonic chiral Landau levels in an elastic metamaterial, Phys. Rev. B **111**, 184303 (2025).
[9] H. Jia, M. Wang, S. Ma, R.-Y. Zhang, J. Hu, D. Wang, and C. T. Chan, Experimental realization of chiral Landau levels in two-dimensional Dirac cone systems with inhomogeneous effective mass, Light Sci. Appl. **12**, 165 (2023).
[10] Z. Cui, C. Wu, Q. Wei, M. Yan, and G. Chen, On-chip elastic wave manipulations based on synthetic dimension, Phys. Rev. Lett. **133**, 256602 (2024).
[11] S. Li, P. G. Kevrekidis, and J. Yang, Emergence of elastic chiral Landau levels and snake states, Phys. Rev. B **109**, 184109 (2024).
[12] L. Fan, Z. Lan, Y. Chen, J. Zhu, and Z. Su, Dual-band flexible large-area ultrasonic energy conveying via elastic chiral Landau levels, Mater. Horiz. **12**, 6334 (2025).
[13] X. Wen, C. Qiu, Y. Qi, L. Ye, M. Ke, F. Zhang, and Z. Liu, Acoustic Landau quantization and quantum-Hall-like edge states, Nat. Phys. **15**, 352 (2019).
[14] M. Barsukova, F. Grisé, Z. Zhang, S. Vaidya, J. Guglielmon, M. I. Weinstein, L. He, B. Zhen, R. McEntaffer, and M. C. Rechtsman, Direct observation of Landau levels in silicon photonic crystals, Nat. Photonics **18**, 580 (2024).
[15] C. Brendel, V. Peano, O. J. Painter, and F. Marquardt, Pseudomagnetic fields for sound at the nanoscale, Proc. Natl. Acad. Sci. U.S.A. **114**, e3390 (2017).
[16] M. Yan, W. Deng, X. Huang, Y. Wu, Y. Yang, J. Lu, F. Li, and Z. Liu, Pseudomagnetic fields enabled manipulation of on-chip elastic waves, Phys. Rev. Lett. **127**, 136401 (2021).
[17] R. Barczyk, L. Kuipers, and E. Verhagen, Observation of Landau levels and chiral edge states in photonic crystals through pseudomagnetic fields induced by synthetic strain, Nat. Photonics **18**, 574 (2024).
[18] M. C. Rechtsman, J. M. Zeuner, A. Tünnermann, S. Nolte, M. Segev, and A. Szameit, Strain-induced pseudomagnetic field and photonic Landau levels in dielectric structures, Nat. Photonics **7**, 153 (2013).
[19] H. Abbaszadeh, A. Souslov, J. Paulose, H. Schomerus, and V. Vitelli, Sonic Landau levels and synthetic gauge fields in mechanical metamaterials, Phys. Rev. Lett. **119**, 195502 (2017).
[20] Y. Chen, Z. Lan, S. Liang, L. Fan, J. Zhu, and Z. Su, Realization of spin-locked acoustic helical Landau levels in both hexagonal and square lattices, Adv. Sci. **12**, e07059 (2025).
[21] Y. Liu, K. Li, W. Liu, Z. Zhang, Y. Cheng, and X. Liu, Observation of chiral Landau levels in two-dimensional acoustic system, Quantum Front. **3**, 1 (2024).
[22] Y. Chen, Z. Lan, S. Liang, S.-k. C. Cheung, L. Fan, J. Zhu, and Z. Su, Visualization of flexible large-area acoustic energy conveying enabled by valley-dependent Landau bulk modes, Sci. China Phys. Mech. Astron. **68**, 1 (2025).
[23] Z. Yang, F. Gao, Y. Yang, and B. Zhang, Strain-induced gauge field and Landau levels in acoustic structures, Phys. Rev. Lett. **118**, 194301 (2017).

[24] P. Li, W. Chen, J. Chen, W. Luo, and D. Zhao, Acoustic Landau levels in a synthetic magnetic field with a symmetric gauge, Phys. Rev. Appl. **22**, 014047 (2024).
[25] B. Yang, X. Shen, L. Shi, Y. Yang, and Z. H. Hang, Nonuniform pseudo-magnetic fields in photonic crystals, Adv. Photonics Nexus **3**, 026011 (2024).
[26] J.-W. Rhim and Y. B. Kim, Landau level quantization and almost flat modes in three-dimensional semimetals with nodal ring spectra, Phys. Rev. B **92**, 045126 (2015).
[27] M.-C. Jin, Z.-G. Chen, M.-H. Lu, P. Zhan, and Y.-F. Chen, Flat Landau levels and interface states in two-dimensional photonic crystals with a nodal ring, Phys. Rev. B **109**, 054108 (2024).
[28] Z. Cheng, Y.-J. Guan, H. Xue, Y. Ge, D. Jia, Y. Long, S.-Q. Yuan, H.-X. Sun, Y. Chong, and B. Zhang, Three-dimensional flat Landau levels in an inhomogeneous acoustic crystal, Nat. Commun. **15**, 2174 (2024).
[29] X. Zhang, L. Liang, K. Shao, F. Li, B. Jin, H. Wang, Y. Poo, W. Chen, and C. T. Chan, Photonic flat Landau levels induced by antisymmetric nonuniform pseudomagnetic fields, Phys. Rev. Lett. **135**, 176602 (2025).
[30] W. Zhao, Y. Zheng, C. Lu, Z. Wang, Y.-C. Liu, and S. Zhang, Landau rainbow induced by artificial gauge fields, Phys. Rev. Lett. **133**, 233801 (2024).
[31] S. El Soliman, M. Barlou, Z. J. Wong, and K. L. Tsakmakidis, Topological rainbow trapping, Nat. Rev. Phys. **7**, 409 (2025).
[32] S. E. Soliman, B. Maria, K. L. Tsakmakidis, and Z. J. Wong, Rainbow trapping for advanced wave control, Adv. Phys. X **10**, 2517551 (2025).
[33] Y. Chen, L. Fan, J. Zhu, L. An, and Z. Su, Rainbow energy harvesting using a high-order topological meta-device, Nano Energy **127**, 109722 (2024).
[34] Z.-D. Zhang, S.-Y. Yu, M.-H. Lu, and Y.-F. Chen, Gigahertz surface acoustic wave topological rainbow in nanoscale phononic crystals, Phys. Rev. Lett. **133**, 267001 (2024).
[35] G. Duan, S. Zheng, Z. Cheng, H. Wu, and B. Xia, Gear fault detection via deep-subwavelength rainbow trapping effect of higher-order topological mechanical metamaterials, Adv. Funct. Mater. **35**, 2425815 (2025).
[36] C. Xu, G. Ma, Z.-G. Chen, J. Luo, J. Shi, Y. Lai, and Y. Wu, Three-dimensional acoustic double-zero-index medium with a fourfold degenerate Dirac-like point, Phys. Rev. Lett. **124**, 074501 (2020).
[37] C. Xu, H. Chu, J. Luo, Z.-H Hang, Y. Wu, and Y. Lai, Three-dimensional electromagnetic void space, Phys. Rev. Lett. **127**, 123902 (2021).
[38] C. Xu, J. Shi, X. Liu, Z.-G Chen, Y. Wu, and Y. Lai, Deterministic double-zero media and robust wave manipulation using a phononic Weyl semimetal, Phys. Rev. Lett. **135**, 046902 (2025).
[39] See Supplemental Material at http://link.aps.org/supplemental/10.1103/rt58-kxy9 for the decoupling of out-of-plane and in-plane polarized elastic waves, detailed geometry parameters of the cladding layers, tight-binding model of the flat Landau levels and Landau rainbow, effect of the number of unit cells within the PMF domain on the degeneracy of the zeroth Landau levels, computational details about the full-wave simulations, effect of possible fabrication errors on the fields of the Landau rainbow and experimental details for characterizing the Landau rainbow, which includes Refs. [40–42].
[40] H. Fan, B. Xia, L. Tong, S. Zheng, and D. Yu, Elastic higher-order topological insulator with topologically protected corner states, Phys. Rev. Lett. **122**, 204301 (2019).
[41] S. Hedayatrasa, K. Abhary, M. Uddin, and C.-T. Ng, Optimum design of phononic crystal perforated plate structures for widest bandgap of fundamental guided wave modes and maximized in-plane stiffness, J. Mech. Phys. Solids **89**, 31 (2016).
[42] S. Hedayatrasa, M. Kersemans, K. Abhary, M. Uddin, J. K. Guest, and W. Van Paepegem, Maximizing bandgap width and in-plane stiffness of porous phononic plates for tailoring flexural guided waves: Topology optimization and experimental validation, Mech. Mater. **105**, 188 (2017).
[43] Z.-D. Zhang, S.-Y. Yu, M.-H. Lu, and Y.-F. Chen, Near GHz lithium liobate higher-order topological nanomechanical metamaterials, Nano Lett. **24**, 15421 (2024).
[44] O. Florez, G. Arregui, M. Albrechtsen, R. C. Ng, J. Gomis-Bresco, S. Stobbe, C. M. Sotomayor-Torres, and P. D. García, Engineering nanoscale hypersonic phonon transport, Nat. Nanotechnol. **17**, 947 (2022).
[45] Q. Zhang, D. Lee, L. Zheng, X. Ma, S. I. Meyer, L. He, H. Ye, Z. Gong, B. Zhen, and K. Lai, Gigahertz topological valley Hall effect in nanoelectromechanical phononic crystals, Natl. Electron. Rev. **5**, 157 (2022).
[46] S.-N. Liang, Z.-H. Qin, S.-M. Wu, H.-Y. Chen, S.-Y. Yu, and Y.-F. Chen, Deployable nanoelectromechanical bound states in the continuum in GHz lamb wave phononic crystals on $LiNbO_3$ thin films, Phys. Rev. Lett. **135**, 206201 (2025).
[47] The data used to produce the findings of this study are available via Zenodo at https://zenodo.org/records/18396313.